nium and hydroxide ions.

We describe the solvent coordinate that stabilizes ions, ΔE, as an electric field because it arises primarily from long-range electrostatic interactions. Local properties that we examined, such as ion coordination number and the presence of specific hydrogen bonds, fail to account for the bond-destabilizing fluctuation in our simulations. Furthermore, the stabilization of ions indicated in Fig. 2, B and C, is diminished substantially when we artificially remove outer coordination shells of the ions. Thus, ΔE does not arise from a few nearby water molecules. Instead, it is analogous to the collective coordinates that others have imagined for electron transfer (*10*) and for acid-base proton transfer (*33–36*). As in Marcus's theory of electron transfer, it is a rare solvent fluctuation that drives the motion of charges. In detail, however, ΔE differs from the previously defined coordinates, namely the solvent polarization field and the energy gap between diabatic bonding states. ΔE involves only the energy required to transfer protons adiabatically. The second component of the reaction coordinate that we identified, the hydrogen bond wire length l, is also analogous to a coordinate in these theories, namely the distance between ions. But in the case of autoionization, the appropriate separation coordinate describes the hydrogen bond wires that link the ions, rather than simply describing the distance between them, emphasizing the importance of connectivity in the hydrogen bond network.

We conclude that the dynamics of both electric fields and hydrogen bonding play important roles in the autoionization mechanism. Rare electric field fluctuations drive the dissociation of oxygen-hydrogen bonds. Ions produced in this way usually recombine quickly because the solvation fluctuation vanishes within tens of femtoseconds. But when such a fluctuation is coincident with breaking of the hydrogen bond wire (a process normally occurring about once every picosecond), rapid recombination is then not possible. It is with this coincidence of events that the system crosses a transition state. This scenario implies the existence of many short-lived hydronium and hydroxide ions in water. Decay of this transient population over ~100 fs is an interesting and, in principle, observable signature of the dynamics revealed by our simulations.

References and Notes

1. M. Eigen, L. De Maeyer, *Z. Elektrochem.* **59**, 986 (1955).
2. W. C. Natzle, C. B. Moore, *J. Phys. Chem.* **89**, 2605 (1985).
3. B. L. Trout, M. Parrinello, *J. Phys. Chem. B* **103**, 7340 (1999).
4. ———, *Chem. Phys. Lett.* **288**, 343 (1999).
5. R. Car, M. Parrinello, *Phys. Rev. Lett.* **55**, 2471 (1985).
6. C. Dellago, P. G. Bolhuis, F. S. Csajka, D. Chandler, *J. Chem. Phys.* **108**, 1964 (1998).
7. C. Dellago, P. G. Bolhuis, D. Chandler, *J. Chem. Phys.* **108**, 9236 (1998).
8. P. G. Bolhuis, C. Dellago, D. Chandler, *Faraday Discuss.* **110**, 421 (1998).
9. P. L. Geissler, C. Dellago, D. Chandler, J. Hutter, M. Parrinello, *Chem. Phys. Lett.* **321**, 225 (2000).
10. R. A. Marcus, *J. Chem. Phys.* **24**, 966 (1956).
11. P. L. Geissler, T. Van Voorhis, C. Dellago, *Chem. Phys. Lett.* **324**, 149 (2000).
12. The potential energy required to separate hydronium and hydroxide ions in a cluster of three water molecules was computed by using the BLYP density functional theory and by using a high-level wave function–based method [T. Van Voorhis and P. L. Geissler, unpublished data]. The cluster geometry for these calculations was taken from a wire of hydrogen-bonded molecules present in a bulk water simulation, and protons were placed in a manner similar to that described in (*32*). Both methods predict an energy of ~60 kcal/mol (relative to the neutral cluster) for ions separated by one intervening water molecule. Both also predict similar monotonic decreases in energy as protons are transferred to create neutral water molecules.
13. A. D. Becke, *Phys. Rev. A* **38**, 3098 (1988).
14. C. Lee, W. Yang, R. G. Parr, *Phys. Rev. B* **37**, 785 (1988).
15. J. S. Bader, R. A. Kuharski, D. Chandler, *J. Chem. Phys.* **93**, 230 (1990).
16. D. Marx, M. E. Tuckerman, M. Parrinello, *J. Phys. Condens. Matt.* **12**, 153 (2000).
17. M. Sprik, J. Hutter, M. Parrinello, *J. Chem. Phys.* **105**, 1142 (1996).
18. We calculated the mean force, $F_N(r_{ion})$, exerted on a Na^+Cl^- (aq) ion pair by its environment in a periodically replicated system with N water molecules, as a function of interionic distance, r_{ion}. The model used in these simulations is described in work by P. L. Geissler, C. Dellago, and D. Chandler [*J. Phys. Chem. B* **103**, 3706 (1999)]. We considered N = 30, 106, 254, and 862, corresponding to cell lengths of ~10, 15, 20, and 30 Å, respectively. The resulting functions, $F_N(r_{ion})$, differ by <1 kcal/mol per angstrom.
19. C. Dellago, P. G. Bolhuis, D. Chandler, *J. Chem. Phys.* **111**, 6617 (1999).
20. M. M. Klosek, B. J. Matkowsky, Z. Schuss, *Ber. Bunsenges. Phys. Chem.* **95**, 331 (1991).
21. V. Pande, A. Y. Grosberg, T. Tanaka, E. I. Shakhnovich, *J. Chem. Phys.* **108**, 334 (1998).
22. C. J. T. de Grotthuss, *Ann. Chim.* **58**, 54 (1806).
23. N. Agmon, *Chem. Phys. Lett.* **244**, 456 (1995).
24. M. Tuckerman, K. Laasonen, M. Sprik, M. Parrinello, *J. Chem. Phys.* **103**, 150 (1995).
25. R. Vuilleumier, D. Borgis, *J. Chem. Phys.* **111**, 4251 (1999).
26. U. W. Schmitt, G. A. Voth, *J. Chem. Phys.* **111**, 9361 (1999).
27. F. H. Stillinger, *Adv. Chem. Phys.* **31**, 1 (1975).
28. D. C. Rapaport, *Mol. Phys.* **50**, 1151 (1983).
29. S.-H. Chen, J. Teixeira, *Adv. Chem. Phys.* **64**, 1 (1986).
30. M. Eigen, *Angew. Chem. Int. Ed. Engl.* **3**, 1 (1964).
31. Z. Luz, S. Meiboom, *J. Am. Chem. Soc.* **86**, 4768 (1964).
32. Supplemental information on this calculation is available at www.sciencemag.org/cgi/content/full/291/5511/2121/DC1.
33. R. R. Dogonadze, A. M. Kuznetsov, V. G. Levich, *Electrochim. Acta* **13**, 1025 (1966).
34. R. A. Marcus, *Proc. Electrochem. Soc.* **80**, 1 (1979).
35. D. Borgis, S. Lee, J. T. Hynes, *Chem. Phys. Lett.* **162**, 19 (1989).
36. K. Ando, J. T. Hynes, *Adv. Chem. Phys.* **110**, 381 (1999).

37. In its initial stages, this research was supported by a Laboratory Directed Research and Development grant at Lawrence Berkeley National Laboratory under U.S. Department of Energy (DOE) contract DE-AC03-76SF00098. It was completed with support from DOE grant DE-FG03-99ER14987. Some of the calculations in this work were performed on an RS/6000 SP large-scale server, which was provided through an IBM Shared University Research grant. P.L.G. was an NSF Predoctoral Fellow. We are grateful to F. Stillinger for providing suggestions for improving the preprint of this paper.

30 October 2000; accepted 29 January 2001

Photoinduction of Fast, Reversible Translational Motion in a Hydrogen-Bonded Molecular Shuttle

Albert M. Brouwer,[1] Céline Frochot,[1] Francesco G. Gatti,[2] David A. Leigh,[2]* Loïc Mottier,[3] Francesco Paolucci,[3] Sergio Roffia,[3] George W. H. Wurpel[1]*

A rotaxane is described in which a macrocycle moves reversibly between two hydrogen-bonding stations after a nanosecond laser pulse. Observation of transient changes in the optical absorption spectrum after photoexcitation allows direct quantitative monitoring of the submolecular translational process. The rate of shuttling was determined and the influence of the surrounding medium was studied: At room temperature in acetonitrile, the photoinduced movement of the macrocycle to the second station takes about 1 microsecond and, after charge recombination (about 100 microseconds), the macrocycle shuttles back to its original position. The process is reversible and cyclable and has properties characteristic of an energy-driven piston.

Analogic molecular versions of some of the fundamental components of machinery from the macroscopic world are currently being targeted as prototypical structural units for devices that could function through mechanical motion at the molecular level (*1–5*). A common design feature behind such structures is that the architectures are chosen so as

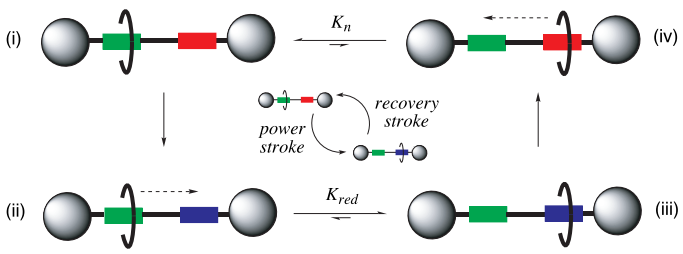

Scheme 1. Translational submolecular motion in a stimuli-responsive molecular shuttle: (i) The macrocycle initially resides at the preferred (green) station; (ii) a reaction occurs (red → blue) changing the relative binding potentials of the two stations such that (iii) the macrocycle "shuttles" to the now-preferred (blue) station. In the special case that the reverse reaction (blue → red) now occurs (iv), the components return to their original positions. Such cyclable, externally driven, mechanical motions with a "power stroke" and a "recovery stroke" are reminiscent of the workings of a simple piston (inset).

to restrict the degrees of freedom of submolecular components such that they can only move with respect to each other through discrete, large-amplitude internal motions, preferably under external influences. In rotaxanes, molecules where a macrocyclic "bead" is locked onto a linear "thread" by bulky "stoppers" (*6*), such controlled dynamic behavior occurs if the macrocycle can be induced to move from one initially favored position ("station") on a thread to a second site where preferential binding of the macrocycle results as a consequence of some external stimuli [a responsive "molecular shuttle" (*7*–*14*), Scheme 1].

Here we report an example of a hydrogen-bond (H-bond)–assembled rotaxane in which translation of the macrocycle between two stations takes place after photoexcitation with a laser pulse (Scheme 2) (*14*). The submolecular motion is fast (~1 μs; previous light-driven shuttles generally function on the time scale of minutes to hours) (*10*, *12*), fully reversible, and, remarkably, can be observed directly by following transient changes in the optical absorption spectrum. After charge recombination, ~100 μs later, the macrocycle shuttles back to its original site. The whole process is cyclable and reminiscent of the workings of a piston, where a powered stroke (during which mechanical work can be performed) is followed by a recovery stroke that returns the system to its starting position (inset, Scheme 1) (*15*).

The molecular shuttle **1** consists of a benzylic amide macrocycle mechanically locked onto a thread, **2**, featuring two potential H-bonding stations—a succinamide (*succ*) site and a 3,6-di-*tert*-butyl-1,8-naphthalimide (*ni*) unit—separated by a C_{12} alkyl spacer (Fig. 1).[1] Succinamide units have H-bond–accepting sites in identical positions to dipeptides, and, in nonpolar solvents, threads containing such motifs template the formation of benzylic amide macrocycles about them to give rotaxanes in five component "clipping" reactions (*16*). Thus, treatment of **2** with 10 equivalents each of xylylene diamine and isophthaloyl dichloride ($CHCl_3$, Et_3N, 4 hours, high dilution) led to the formation of the [2]rotaxane **1** in 59% yield.

X-ray crystal structures (*17*) of model succinamide rotaxanes show the *succ* station to be an excellent fit for the benzylic amide macrocycle binding sites, held in place by two sets of bifurcated H-bonds from the isophthalamide groups of the macrocycle to the two succinamide amide carbonyls. In the neutral state, naphthalimide is a poor H-bond acceptor (*18*), and therefore in solvents that do not disrupt H-bonds, the rotaxane must minimize its energy by adopting the co-conformation (*19*) and H-bonding motif shown as *succ*-**1** in Scheme 2. As a radical anion, however, naphthalimide has a greatly enhanced H-bond–accepting affinity (*18*) and the photo- or electrochemically reduced form of the *ni* station can therefore bind strongly to the benzylic amide macrocycle. This differential binding potential provides a driving force for it to shuttle down the thread from its original position (Scheme 2).

Confirmation that the equilibrium (K_n) lies almost completely toward *succ*-**1** in the neutral rotaxane was provided by a variety of spectroscopic and physical methods. The ^1H nuclear magnetic resonance (NMR) spectrum of **1** in d_3-MeCN (Fig. 2) shows an upfield shift of 1.2 parts per million for the methylene protons (H_d and H_e) of the succinamide station relative to the same signals in **2** due to binding of the macrocycle (the shielding is caused by the field effects of the aromatic rings of the xylylene residues). In contrast, the chemical shifts of the resonances of the naphthalimide unit (H_i and H_j) and *N*-meth-

[1]Laboratory of Organic Chemistry, University of Amsterdam, Nieuwe Achtergracht 129, NL-1018 WS Amsterdam, Netherlands. [2]Centre for Supramolecular and Macromolecular Chemistry, Department of Chemistry, University of Warwick, Coventry CV4 7AL, UK. [3]Dipartimento di Chimica "G. Ciamician," Università degli Studi di Bologna, V. F. Selmi 2, 40126, Bologna, Italy.

*To whom correspondence should be addressed. E-mail: David.Leigh@Warwick.ac.uk and fred@org.chem.uva.nl

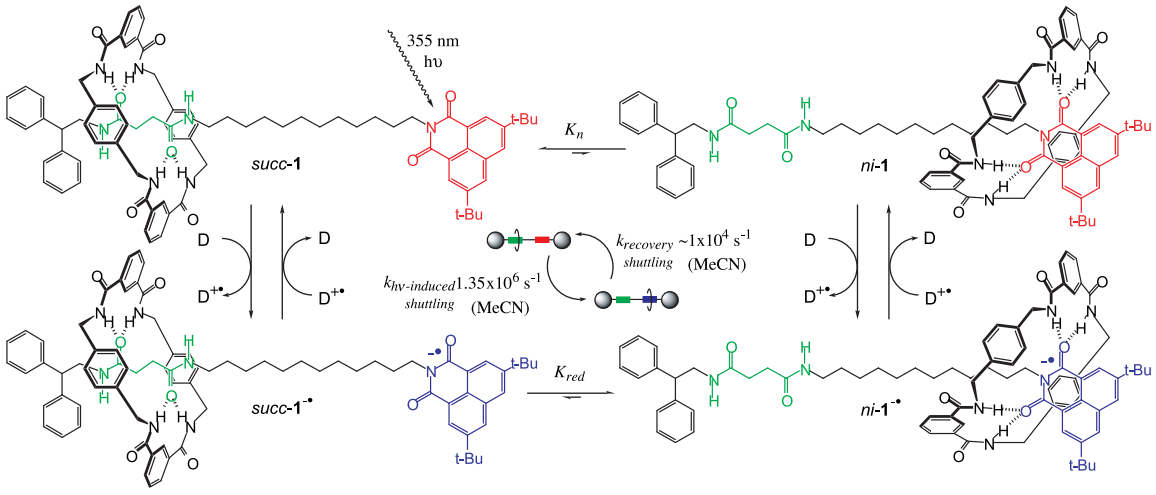

Scheme 2. A photoresponsive, H-bond–assembled, molecular shuttle **1**. Before the 355-nm laser pulse, the translational co-conformer *succ*-**1** is predominant because the *ni* station is a poor H-bond acceptor (K_n < 0.01). After photoreduction by an external donor (D; DABCO, TMPD, or biphenyl), the equilibrium between *succ*-$\mathbf{1}^{\bullet-}$ and *ni*-$\mathbf{1}^{\bullet-}$ changes (K_{red} >1500) because *ni*$^{\bullet-}$ is a powerful H-bond acceptor and back-electron transfer is slow (spin forbidden). Because the absorption maximum (λ_{max}) of *ni*-$\mathbf{1}^{\bullet-}$ is located at shorter wavelength than that of *succ*-$\mathbf{1}^{\bullet-}$, the sum of the absorptions shifts to the blue. The rate at which the absorption shifts (k_{shift}) is related to the rate of change in the relative populations of *succ*-$\mathbf{1}^{\bullet-}$ and *ni*-$\mathbf{1}^{\bullet-}$, i.e., the time taken for light-induced shuttling of the macrocycle (~1 μs, MeCN). After charge recombination (~100 μs, MeCN), the macrocycle shuttles back to its original position. Cycling of this process at 10^4 times per second generates ~10^{-15} W of mechanical power for each shuttle.

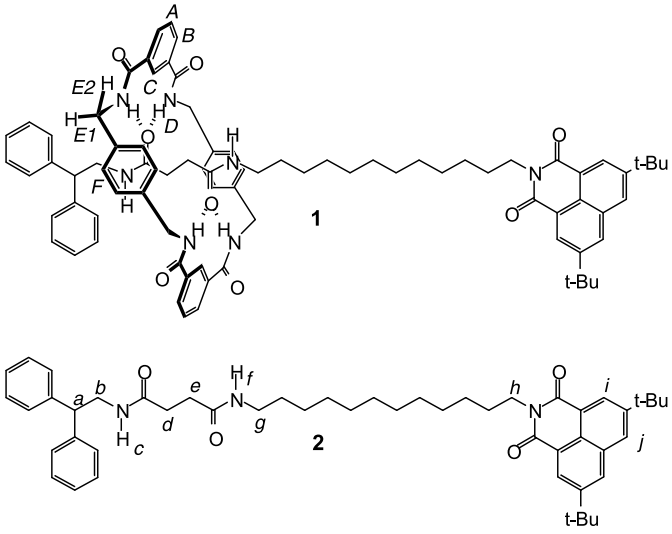

Fig. 1. Chemical formulae of molecular shuttle **1**, shown in its preferred (*succ*-**1**) co-conformation in non–H-bond–disrupting solvents, and thread **2**. The letters identify nonequivalent ^{1}H environments.

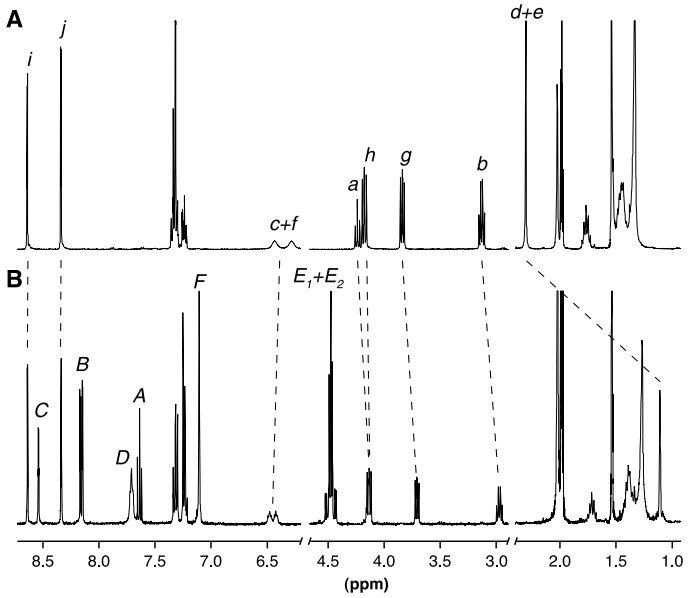

Fig. 2. ^{1}H NMR spectra (400 MHz) of (**A**) **2** and (**B**) **1** in d_3-MeCN at 329 K (**1** is only sparingly soluble in d_3-MeCN at 298 K). The letters correspond to the assignment of the resonances shown in Fig. 1.

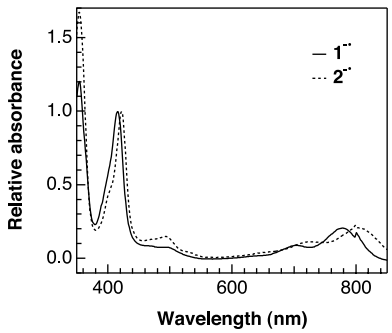

Fig. 3. Electronic absorption spectra of electrochemically generated $\mathbf{1}^{-\cdot}$ and $\mathbf{2}^{-\cdot}$ in DMF at 298 K (corresponding to the largest charge before the isosbestic points were lost). The spectra were normalized to the intense absorption peak in the visible part of the spectrum.

ylene group (H_h) are virtually identical in **1** and **2**. Similarly, the infrared (IR) spectrum of **1** in MeCN shows no changes in the CO stretch vibrations of the naphthalimide moiety compared with **2**. Comparative NMR shielding effects on model rotaxanes and cyclic voltammetry (CV) studies both show that $K_n < 0.01$ for **1** in a range of solvents (CV suggests a K_n as low as 10^{-5} in tetrahydrofuran at 298 K) (*20*).

Translocation of the macrocycle between the *succ* and *ni* stations in the reduced rotaxane was demonstrated by spectroelectrochemistry. After electrochemical reduction [dimethylformamide (DMF), 298 K] of **1** and **2**, the absorption maxima characteristic of the naphthalimide radical anions were found at 415 and 422 nm, respectively (Fig. 3). The shorter wavelength absorption of the napthalimide radical anion reflects increased polarity of its environment (as observed for the thread in various solvents, see below), and the difference in the $ni^{-\cdot}$ absorption wavelength of **1** and **2** is consistent with H-bonding of the macrocycle to the $ni^{-\cdot}$ station in the reduced form of **2**. In the CV experiments, reoxidation of $ni^{-\cdot}$ to *ni* occurs at a much more positive potential in the rotaxane **2** than in the thread **1** (*20*). The difference in the oxidation potentials of **1** and **2**, 0.48 V, is remarkable [redox-active host-guest complexes involving up to three H-bonds to similar naphthalimide units typically give stabilizations of around 0.2 V (*18*, *21*)] and provides a direct measure of the intercomponent binding energy in structure *ni*-$\mathbf{1}^{-\cdot}$ (Scheme 2). This value, 11.2 kcal mol^{-1}, is the equivalent of four strong or three extremely strong H-bonds (OCNH $\cdots$ O=CNR H-bond strengths are in the range 2 to 5 kcal mol^{-1}) (*22*). Molecular modeling shows that such multipoint H-bonding cannot arise from simple folding and requires the macrocycle to physically shuttle down the thread from the succinamide station to the reduced naphthalimide unit to bind efficiently. Model rotaxanes in which the thread amide groups are methylated (so that all of the H-bonds to the $ni^{-\cdot}$ station must come from the macrocycle), or cannot fold for steric reasons, display similar behavior to **1** (*23*). The CV data show that the coconformer equilibrium in the reduced form of **1** lies almost completely toward *ni*-$\mathbf{1}^{-\cdot}$ ($K_{red} > 1500$, Scheme 2).

Reduction of the naphthalimide station could also be achieved with photoinduced electron transfer, initiated by a nanosecond laser pulse, and, remarkably, the changes in the $ni^{-\cdot}$ absorption spectra can be used to measure directly the rate at which the macrocycle shuttles along the thread.

After photoexcitation, the *ni* chromophore in thread **2** or rotaxane **1** undergoes intersystem crossing to the triplet (T) state in high yield (Eq. 1) (*24*). The triplet species have strong absorption bands (*25*) and are readily observed in transient absorption experiments. Upon reduction of the triplets by an electron donor [D, for example, 1,4-diazabicyclo[2.2.2]octane (DABCO, 1 to 10 mM)], contact radical ion pairs are formed. As a result, the *ni* T-T absorption decays more rapidly and a sharp absorption around 416 nm rises together with weaker bands around 490, 730, and 820 nm. These new absorptions are characteristic of a naphthalimide radical anion and consistent with the spectroelectrochemical results. Because back electron transfer is spin forbidden and thus slow, the ion pair can efficiently dissociate (Eq. 2) and the naphthalimide radical anion absorption can thus be observed for >100 μs as it decays by charge recombination (Eq. 3). The photoreduction quantum yield is ~20%.

$$ni \rightarrow {}^1ni^* \rightarrow {}^3ni^* \quad (1)$$

$${}^3ni^* + D \rightarrow {}^3(ni^{-\cdot}D^{+\cdot}) \rightarrow ni^{-\cdot} + D^{+\cdot} \quad (2)$$

$$ni^{-\cdot} + D^{+\cdot} \rightarrow ni + D \quad (3)$$

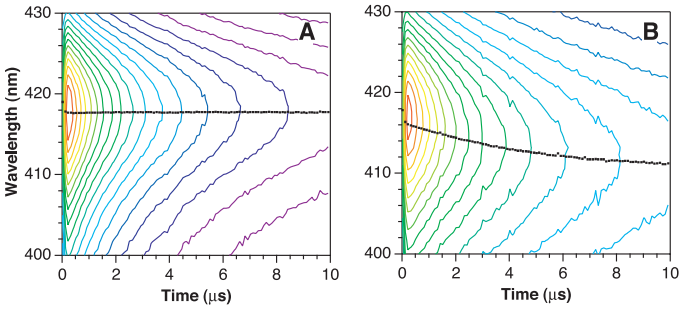

Fig. 4. Contour plots of 100 transient absorption spectra of (**A**) **2** and (**B**) **1** in PrCN with 10 mM DABCO, taken with 100-ns increments after the laser pulse. Optical density decreases from maximum (red) to 0 (blue). The absorption maximum of $ni^{-\cdot}$ is indicated by the black dots and remains constant in thread **2**, whereas it shifts to shorter wavelength for the shuttle **1**.

DABCO was chosen as the electron donor because it has a kinetically stable radical cation with a relatively weak absorption that does not obscure the absorption band of $ni^{-\cdot}$. The radical anion absorption around 416 nm shows a decay that can be fitted to a second order rate law. Most probably, $ni^{-\cdot}$ is converted to *ni* upon bimolecular charge recombination with a donor radical cation. The recombination rate is similar for **1** and **2** ($k = 9 \pm 2 \times 10^9$ M^{-1} s^{-1}). After charge recombination (about 100 μs) the system returns to the ground state and can be pulsed again, giving the same results.

During the lifetime of the naphthalimide radical anion, the position of its absorption maximum located around 416 nm stays constant for the thread (**2**) (Fig. 4A). In the corresponding rotaxane (**1**), however, a blue shift of several nanometers occurs on a microsecond time scale (Fig. 4B) with the magnitude of the photoinduced shift corresponding well to the difference in absorption maxima for $\mathbf{1}^{-\cdot}$ and $\mathbf{2}^{-\cdot}$ measured spectroelectrochemically (Fig. 3). Remarkably, the transient nature of the blue shift of the naphthalimide radical anion absorption maximum is apparently caused by the translation of the macrocycle along the thread to its new equilibrium position, K_{red}. If so, then the rate at which the new equilibrium is established photochemically (that is, the rate of photoinduced shuttling, $k_{h\upsilon\text{-shuttling}}$, Scheme 2) should be related to the rate at which the absorption maximum shifts. This correlation was used both to establish the kinetics of the shuttling process and to provide further evidence that shuttling is, indeed, the process occurring in **1**.

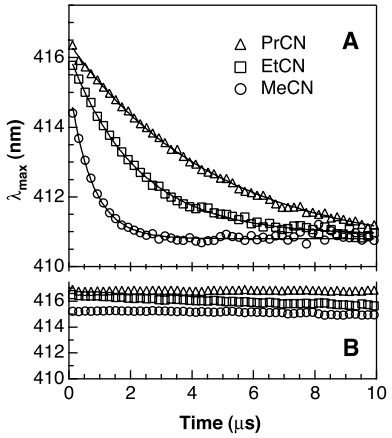

Fig. 5. Changes in the absorption maximum (λ_{max}) of $ni^{-\cdot}$ with time, formed after photoexcitation of (**A**) **1** and (**B**) **2** in the presence of 10 mM DABCO measured in butyronitrile (△), propionitrile (□), and acetonitrile (○). For clarity, half of the data points are omitted. The data for **1** were fitted to a weighted monoexponential function to obtain k_{shift}.

We define the separation between the absorption maxima of free and complexed naphthalimide radical anion as Δλ. Because Δλ is ~5 nm and the absorptions have a full-width at half-maximum (FWHM) > 25 nm, a coalesced band is observed characterized by its maximum λ_{max}. As the relative intensities of the underlying bands change in time, λ_{max} will also change. λ_{max} is linearly correlated to the intensity changes of the separate bands when Δλ is small compared with the width of the separate bands (*26*). Because that is the case here, the measured shift rate of the radical anion absorption maximum (k_{shift}) equals the rate at which the equilibrium for the reduced state is established. Because this lies almost completely toward *ni*-$\mathbf{1}^{-\cdot}$, the rate observed is the macroscopic rate for the translation of the macrocycle along the thread. Indeed, plots of λ_{max} versus time for **1** show perfect monoexponential behavior (Fig. 5).

If, as expected, the rate-determining step for the translational process involves the breaking of the H-bonds between the macrocycle and the *succ* station, then the macrocycle should shuttle more slowly in solvents with a lower dielectric constant (ε) (*11*).

When **1** was photoreduced in the presence of DABCO in alkylnitriles of different polarities, the shift rate indeed followed the predicted trend (Fig. 5): $k_{shift} = 1.35 \times 10^6$ s^{-1} in MeCN (ε = 37.5), 0.45×10^6 s^{-1} in EtCN (ε = 27.2), and 0.21×10^6 s^{-1} in PrCN (ε = 23.3). Similarly, with 3% aqueous MeCN, the rate increased by a factor of 1.5 compared with anhydrous MeCN.

H-bonds are electrostatic in nature, and the free energy of binding of the macrocycle to a station should be inversely proportional to the dielectric constant of the surrounding medium. Therefore, a plot of ln k_{shift} versus 1/ε should yield a linear relation. As demonstrated in Fig. 6A, this is indeed the case. By measuring k_{shift} at different temperatures in PrCN and applying Eyring's transition state theory, the barrier $\Delta G^{\ddagger}$ for the photoinduced translational process in **1** could be determined. A straight line fit of ln k_{shift} versus T^{-1} (Fig. 6B) yielded $\Delta G^{\ddagger} = 10.2 \pm 0.7$ kcal mol^{-1} at 298 K. Similar barriers have been determined by NMR measurements [$\Delta G^{\ddagger}_{298K} = 12.4 \pm 0.3$ kcal mol^{-1} (*11*)] and quantum calculations [$\Delta G^{\ddagger}_{298K} = 11.67$ kcal mol^{-1} (*27*)] for a rotaxane with two glycylglycine H-bond–accepting stations (which has a similar binding motif to succinamide) separated by a 14-atom spacer.

Intramolecular motions after photoexcitation of organic (*28*) and organometallic molecules (*29*) rarely exceed about 1 Å (*30*), as opposed to ~15 Å in the present case. The rate of photoinduced shuttling for **1** lies on the microsecond time scale and can be understood by the ease with which the macrocycle can be dissociated from its initial binding site and the distance it has to travel to the second station. The rate at which the process can be cycled depends on the rate of charge recombination of the rotaxane radical anion. The energy available for the shuttling motion upon reduction of *ni* (power stroke) is about 4.3 kcal mol^{-1} (based on the difference in oxidation potentials of $ni^{-\cdot}$ in **2** versus **1**), and in the reversed direction (recovery stroke), another 6.9 kcal mol^{-1} (based on K_n) is released. If the shuttle is pumped by a laser at the frequency of its recovery stroke (10^4 s^{-1}), the molecular "machine" thus generates ~10^{-15} W of mechanical power per molecule. By comparison, the linear biological "motor" kinesin carries out mechanical work of (48 pN × nm) at 100 steps per second,

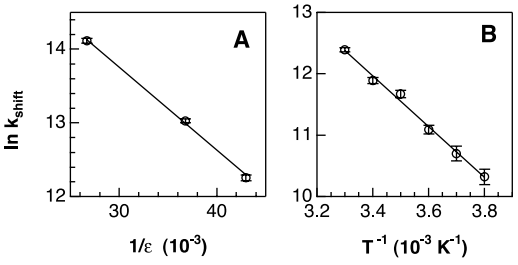

Fig. 6. The dependence of k_{shift} on (**A**) the relative dielectric constant, ε, of the surrounding medium and (**B**) temperature. Error bars indicate the 95% confidence limit.

generating 4.8×10^{-18} W per molecule (*31*). The reason that the synthetic system can do more work than the biomolecular one is that kinesin uses adenosine triphosphate as an energy source, which upon hydrolysis releases ~12 kcal mol^{-1}, whereas the present shuttle uses a 355-nm photon of 81 kcal mol^{-1}.

Tuning of the binding properties of the macrocycle and/or stations, and the photophysical properties of the active chromophore, may allow the use of light of a longer wavelength, faster switching times, and/or more powerful and efficient analogs to be produced. Practical applications of such light-induced mechanical motion at the molecular level might involve the rearrangement of the structure of surfaces or the "fetching-and-carrying" of molecules or clusters of atoms between specific locations (for example, across membranes).

References and Notes

1. For examples, see (*2–5*).
2. V. Balzani, A. Credi, F. M. Raymo, J. F. Stoddart, *Angew. Chem. Int. Ed.* **39**, 3348 (2000).
3. J. K. Gimzewski *et al.*, *Science* **281**, 531 (1998).
4. T. R. Kelly, H. De Silva, R. A. Silva, *Nature* **401**, 150 (1999).
5. N. Koumura, R. W. J. Zijlstra, R. A. van Delden, N. Harada, B. L. Feringa, *Nature* **401**, 152 (1999).
6. J.-P. Sauvage, C. Dietrich-Buchecker, Eds., *Molecular Catenanes, Rotaxanes and Knots* (Wiley-VCH, Weiheim, Germany, 1999).
7. For examples, see (*8–13*).
8. R. A. Bissell, E. Córdova, A. E. Kaifer, J. F. Stoddart, *Nature* **369**, 133 (1994).
9. J.-P. Collin, P. Gaviña, J.-P. Sauvage, *New J. Chem.* **21**, 525 (1996).
10. H. Murakami, A. Kawabuchi, K. Kotoo, M. Kunitake, N. Nakashima, *J. Am. Chem. Soc.* **119**, 7605 (1997).
11. A. S. Lane, D. A. Leigh, A. Murphy, *J. Am. Chem. Soc.* **119**, 11092 (1997).
12. N. Armaroli *et al.*, *J. Am. Chem. Soc.* **121**, 4397 (1999).
13. P. R. Ashton *et al.*, *Chem. Eur. J.* **6**, 3558 (2000).
14. For photoresponsive shuttles, see (*10*, *12*, *13*). For reviews of photoresponsive rotaxanes in general, see A. C. Benniston [*Chem. Soc. Rev.* **25**, 427 (1996)] and M.-J. Blanco *et al.* [*Chem. Soc. Rev.* **28**, 293 (1999)].
15. Some supramolecular complexes that are dethreaded by light have been described as "pistonlike. . . light-fueled motors"; see P. R. Ashton *et al.*, *J. Am. Chem. Soc.* **120**, 11190 (1998); M. Asakawa *et al.*, *Chem. Eur. J.* **5**, 860 (1999).
16. D. A. Leigh, A. Murphy, J. P. Smart, A. M. Z. Slawin, *Angew. Chem. Int. Ed. Engl.* **36**, 728 (1997).
17. Details of crystallographic structures are given in the supplementary material (*32*).
18. A. Niemz, V. M. Rotello, *Acc. Chem. Res.* **32**, 44 (1999).
19. "Co-conformation" refers to the relative positions and orientations of the mechanically interlocked components with respect to each other [M. C. T. Fyfe *et al.*, *Angew. Chem. Int. Ed. Engl.* **36**, 2068 (1997)].
20. Details of the CV behavior of **1** and **2** can be found in the supplementary material (*32*).
21. Y. Ge, R. R. Lilienthal, D. K. Smith, *J. Am. Chem. Soc.* **118**, 3976 (1996).
22. G. A. Jeffrey, *An Introduction to Hydrogen Bonding* (Oxford Univ. Press, New York, 1997).
23. Further physical and spectroscopic evidence that rule out folding being the dominant photoinduced process occurring in **1** are provided as supplementary material (*32*).
24. Selective photoexcitation with the third harmonic of a Q-switched Nd:yttrium-aluminum-garnet laser (355 nm, FWHM = 2 ns) of the *ni*-chromophore in **2** leads to the prompt appearance of the triplet-triplet absorption, with characteristic peaks at 369, 441 (shoulder), and 467 nm in MeCN. The decay of the triplet is nonexponential but becomes nearly monoexponential when using the lowest possible laser power on a dilute sample. Under these conditions, the triplet state has a decay time of 43 μs in MeCN. The time resolution of our transient absorption setup (5 ns) does not allow for the detection of the short-lived singlet state. Time-correlated single photon counting, however, afforded a value for the fluorescence decay time of τ_f = 1.6 ns (MeCN).
25. V. Wintgens *et al.*, *J. Chem. Soc. Faraday Trans.* **90**, 411 (1994).
26. Proof of the linear relation between λ_{max} and the intensity of the separate bands when $\Delta\lambda$ is small compared with the width of the separate bands can be found in the supplementary material (*32*).
27. D. A. Leigh, A. Troisi, F. Zerbetto, *Angew. Chem. Int. Ed.* **39**, 350 (2000).
28. D. H. Waldeck, *Chem. Rev.* **91**, 415 (1991).
29. K. M. Omberg *et al.*, *J. Am. Chem. Soc.* **119**, 7013 (1997).
30. X. Y. Lauteslager, I. H. M. van Stokkum, H. J. van Ramesdonk, A. M. Brouwer, J. W. Verhoeven, *J. Phys Chem. A* **103**, 653 (1999).
31. S. M. Block, *Cell* **93**, 5 (1998).
32. Supplementary material is available on *Science* Online at www.sciencemag.org/cgi/content/full/1057886/DC1.

33. This work was supported by the Training and Mobility of Researchers initiative of the European Union through contract FMRX-CT97-0097 (Development of Rotaxane-based Unconventional Materials Network), the Netherlands Organization for Scientific Research (Nederlandse Organisatie voor Wetenschappelijk Onderzoek, NWO) and the Engineering and Physical Sciences Research Council (EPSRC). D.A.L. is an EPSRC Advanced Research Fellow (AF/982324); F.G.G. is a Marie Curie Research Fellow (ERBFMBI-CT97-2834).

29 November 2000; accepted 13 February 2001
Published online 22 February 2001;
10.1126/science.1057886
Include this information when citing this paper.

Tropical Tropospheric Ozone and Biomass Burning

Anne M. Thompson,[1,2]* Jacquelyn C. Witte,[1,4] Robert D. Hudson,[2] Hua Guo,[3] Jay R. Herman,[1] Masatomo Fujiwara[5]

New methods for retrieving tropospheric ozone column depth and absorbing aerosol (smoke and dust) from the Earth Probe–Total Ozone Mapping Spectrometer (EP/TOMS) are used to follow pollution and to determine interannual variability and trends. During intense fires over Indonesia (August to November 1997), ozone plumes, decoupled from the smoke below, extended as far as India. This ozone overlay a regional ozone increase triggered by atmospheric responses to the El Niño and Indian Ocean Dipole. Tropospheric ozone and smoke aerosol measurements from the Nimbus 7 TOMS instrument show El Niño signals but no tropospheric ozone trend in the 1980s. Offsets between smoke and ozone seasonal maxima point to multiple factors determining tropical tropospheric ozone variability.

Smoke and excess tropospheric ozone, both by-products of biomass burning, have long been observed over large regions of the tropics with satellites (*1–3*), aircraft, balloons, and ground-based instrumentation (*4–6*). Ozone forms as a result of biomass burning because combustion products are ozone precursors in the atmosphere: nitrogen oxides, carbon monoxide, and hydrocarbons. Other combustion products lead to the formation of aerosol particles, including soot, that make up smoke. The highest smoke aerosol and tropospheric ozone amounts occur over southern Africa and the adjacent Atlantic (*2*, *5*, *7*), where a strong ozone, biomass-burning link has been confirmed by airborne and ship-based measurements (*5*, *8–11*). However, other observations (*12*) and some models (*13–15*) point to large-scale dynamics and lightning as prominent factors in tropical tropospheric ozone distributions.

Since late 1996, with the launch of Earth Probe–Total Ozone Mapping Spectrometer (EP/TOMS) (*16*), real-time processing of absorbing aerosol (smoke) and tropospheric ozone has enabled daily tracking of these pollutants at 1° latitude by 1.25° longitude resolution. The first exceptional ozone episode detected by EP/TOMS occurred during the 1997 El Niño–Southern Oscillation (ENSO) and Indian Ocean Dipole (IOD) events, when drought over Indonesia was followed by large fires. Here, we use climatological indices to show that ozone variations during this time resulted from perturbed dynamics, as well as from more active photochemistry (*17–21*). Comparison of the EP/TOMS record with data from the Nimbus 7/TOMS instrument that operated from 1979 to 1992 (*7*) shows similarities to data from 1997 and allows determination of seasonal

[1]NASA–Goddard Space Flight Center, Code 916, Greenbelt, MD 20771, USA. [2]Department of Meteorology and [3]Department of Computer Sciences, University of Maryland, College Park, MD 20742, USA; [4]Science Systems and Applications, Lanham, MD 20706, USA; [5]Graduate School of Environmental Earth Science, Hokkaido University, Sapporo 060-0810, Japan.

*To whom correspondence should be addressed: E-mail: anne.m.thompson@gsfc.nasa.gov